

# Fermion determinants in matrix models of QCD at nonzero chemical potential

M.A. Halasz<sup>a</sup>, A.D. Jackson<sup>b</sup> and J.J.M. Verbaarschot<sup>a</sup>

<sup>a</sup> Department of Physics, SUNY, Stony Brook, New York 11794, USA

<sup>b</sup> Niels Bohr Institute, Blegdamsvej 17, Copenhagen, DK-2100, Denmark

## Abstract

The presence of a chemical potential completely changes the analytical structure of the QCD partition function. In particular, the eigenvalues of the Dirac operator are distributed over a finite area in the complex plane, whereas the zeros of the partition function in the complex mass plane remain on a curve. In this paper we study the effects of the fermion determinant at nonzero chemical potential on the Dirac spectrum by means of the resolvent,  $G(z)$ , of the QCD Dirac operator. The resolvent is studied both in a one-dimensional  $U(1)$  model (Gibbs model) and in a random matrix model with the global symmetries of the QCD partition function. In both cases we find that, if the argument  $z$  of the resolvent is not equal to the mass  $m$  in the fermion determinant, the resolvent diverges in the thermodynamic limit. However, for  $z = m$  the resolvent in both models is well defined. In particular, the nature of the limit  $z \rightarrow m$  is illuminated in the Gibbs model. The phase structure of the random matrix model in the complex  $m$  and  $\mu$ -planes is investigated both by a saddle point approximation and via the distribution of Yang-Lee zeros. Both methods are in complete agreement and lead to a well-defined chiral condensate and quark number density.

March 11, 1997

## 1. Introduction

During the past decade, numerical lattice QCD simulations have provided a great deal of insight regarding strong interactions at finite temperature (see [1,2] for a review). In spite of steady progress [3] numerical simulations of QCD at finite baryon density have proved to be remarkably difficult and their results remain inconclusive [4,5]. The main reason for these difficulties can be traced back to the way the quark number chemical potential enters a Euclidean field theory. It results in a fermion determinant and a probability measure that are not positive definite, making standard Monte Carlo simulations impossible. A possible solution to this problem is the quenched approximation, i.e., ignoring the fermion determinant in generating gauge field configurations. This method has been quite successful in other applications of LGT (see e.g., [6]). Unfortunately, results obtained for finite chemical potential show a critical value of  $\mu$  at half the pion mass instead of a third of the nucleon mass [4]. Two possible explanations have been offered in the literature: i) The problems are an artifact of relatively small lattices and would be cured in the continuum limit [7,8]. ii) The quenched approximation is responsible for these unphysical results [9,10]. Regarding the latter point we mention one particularly interesting suggestion [11,12], namely that the quenched approximation is obtained as the limit of the number of flavors going to zero with an equal number of fermions and conjugate fermions, i.e., the limit of a partition function in which only the absolute value of the determinant enters. Recently, this suggestion has been made much more explicit by Stephanov [12] within the framework of a random matrix model with the chiral and flavor structure of the Dirac operator (see [18] for a review). He has shown *analytically* that the quenched Dirac spectrum is obtained in the limit as both the number of quarks and conjugate quarks tend to zero. Remarkably, the chiral condensate of this model (with the full determinant included) is independent of the number of flavors if  $N_f$  is a positive integer. However, since *real* QCD does not have such conjugate quarks, it seems unlikely that its  $N_f \rightarrow 0$  limit would lead to the quenched approximation.

This leads to the more general question regarding the extent to which the quenched approximation can be trusted. Another familiar example of its failure is the chiral limit, in which the quenched theory does not reproduce the correct chiral logarithms [13]. The

failure of the quenched approximation is most obvious if the quark mass is less than the smallest nonzero Dirac eigenvalue. Then the chiral condensate in the full theory is zero for two or more flavors, finite for one flavor and possibly divergent in the quenched approximation [14]. The reason for the failure is that the leading contribution to the expectation value of an operator is a subleading contribution to the partition function. A similar mechanism is at work in one-dimensional  $U(N)$  lattice models [10,15]. There, the leading contribution to the fermion determinant cancels after averaging over the gauge group. This is no longer true if the gauge group is  $SU(N)$ . Then, the chiral condensate in the quenched and unquenched theory are indeed equal [16,7].

The random matrix model studied in this paper is the extension to nonzero chemical potential of the model introduced in [17]. The partition function is defined by

$$Z = \int DHP(H) \det^{N_f}(m - D) , \quad (1)$$

where  $D$  is the random Dirac operator

$$D = \begin{pmatrix} 0 & iW + \mu \\ iW^\dagger + \mu & 0 \end{pmatrix} , \quad (2)$$

and  $W$  is a complex matrix distributed according to the Gaussian probability distribution distribution  $P(W)$

$$P(W) = \exp(-n\Sigma^2 \text{Tr}WW^\dagger) . \quad (3)$$

For nonzero chemical potential, the Euclidean QCD Dirac operator is  $D = \gamma_\mu(\partial_\mu + iA_\mu) + \gamma_0 \mu$ . The random matrix partition function is obtained from the QCD partition function by replacing the  $\mu$ -independent terms of the matrix elements of the Dirac operator in a chiral basis by Gaussian random variables. In this basis, the term  $\mu\gamma_0$  results in the term  $\mu$  times the identity in the off-diagonal blocks in (2). We wish to emphasize that this random matrix model is a *schematic* model of the QCD partition function.

The random matrix model (1) is in the class of nonhermitean random matrix models. Recently, a variety of such models with applications to different physical problems have been discussed in the literature (see for example [20,21]).

The Euclidean Dirac operator at non-zero chemical potential is non-Hermitian, and, in general, its eigenvalues will be distributed in the complex plane. Indeed, this was found

in lattice simulations by the Urbana group [4]. The quenched case is defined as the theory which is obtained by ignoring the fermion determinant in the partition function (1). In [12] it was pointed out that this theory is not obtained by taking the limit  $N_f \rightarrow 0$  in (1), but rather from the partition function (1) with  $\det(m - D)^{N_f}$  replaced by  $|\det(m - D)|^{N_f}$ .

The partition function (1) will be studied with the help of the resolvent defined by

$$G(z) = \frac{1}{N} \langle \text{Tr} \frac{1}{z - D} \rangle \quad (4)$$

where the average is over the probability distribution (3) and the fermion determinant. For  $z = m$ , the singularities of the resolvent will be cancelled by the fermion determinant in (1). This is the physical (unquenched) case.

In this paper we will investigate the resolvent for  $z \neq m$  at nonzero chemical potential. Our main point is that quenching completely changes the result for  $G(z)$ . In particular, we hope to convince the reader that, below a critical value of  $z$ , the thermodynamic limit of  $G(z)$  does not exist if the valence quark mass is (i.e.,  $z$ ) is different from the sea quark mass  $m$ . We shall show this for the  $U(1)$  model introduced by Gibbs [10]. For the random matrix model (1) the resolvent can be obtained analytically only for  $z = m$ . In this case, it is well defined and displays a first-order phase transition at a nonzero critical value of  $\mu$ . However, if valence and sea quark masses are different, numerical evidence shows that the thermodynamic limit of the resolvent is divergent in this model as well.

We start with some general definitions and discuss the relations between the Dirac spectrum and the zeros of the partition function. Two simple models that lead to nonanalyticities in  $G(z)$  are discussed in section 3. In section 4 we analyze the resolvent in the Gibbs model [9,10]. In section 5 the random matrix model (1) is analyzed by means of a saddle point approximation and via the Yang-Lee zeros of the partition function (some of these results have been published in [19]). The quark number density is discussed in section 6. Numerical results for the random matrix resolvent with  $z \neq m$  are presented in section 7, and concluding remarks are made in section 8.

## 2. Generalities

We will study the spectrum of the Dirac operator via the analytic properties of the resolvent (4). All eigenvalues of the Dirac operator (2) occur in pairs  $\pm\Lambda$ . Therefore, the resolvent satisfies

$$G(z) = -G(-z) . \quad (5)$$

If the distribution of the phases of the matrix elements of the Dirac operator over the ensemble is reflection symmetric with respect to the real axis, we also have the relation

$$G(z^*) = G^*(z) . \quad (6)$$

Contrary to (5) this relation is in general only valid after averaging. For a Hermitean Dirac operator, both relations are valid before averaging.

Our central object of interest is the chiral condensate  $\Xi$  defined by

$$\Xi = \lim_{m \rightarrow 0} \Xi(m) , \quad (7)$$

where

$$\Xi(m) = \lim_{N \rightarrow \infty} \frac{1}{NN_f} \partial_m \log Z(m) . \quad (8)$$

The differentiation with respect to  $m$  can be carried out before or after averaging over the gauge field configurations. In the first case, we factorize the fermion determinant as

$$\det(D - m) = \prod_k (m - \lambda_k) \quad (9)$$

resulting in

$$\Xi(m) = \frac{1}{N} \sum_k \frac{1}{m - \lambda_k} \equiv G(m) . \quad (10)$$

According to (5), a nonzero chiral condensate necessarily implies that  $G(m)$  shows a discontinuity at  $m = 0$  along the real axis.

In the second case, we factorize the partition function as

$$Z(m, \mu) = \prod_k (m - m_k) , \quad (11)$$

where the  $m_k$  are the Yang-Lee zeros of the partition function. In this case

$$\Xi(m) = \frac{1}{N_f N} \sum_k \frac{1}{m - m_k} . \quad (12)$$

In the phase of broken chiral symmetry,  $\Xi(m)$  shows a discontinuity at  $m = 0$ . This necessarily implies that the zeros form a cut in the thermodynamic limit.

The quark number density is defined as

$$n_q = \frac{1}{N N_f} \partial_\mu \log Z . \quad (13)$$

Here, too, we can differentiate before or after averaging over the gauge field configurations. In the first case, the quark number density is given by

$$n_q = \frac{1}{N N_f} \sum_k \left\langle \frac{1}{\mu - \zeta_k} \right\rangle , \quad (14)$$

where the  $\zeta_k$  are the eigenvalues of  $\gamma_0(D + m)$ . They are the analogue of the eigenvalues of the propagator matrix introduced by Gibbs [9]. If, on the other hand, we first average over the gauge field configurations, the partition function can be factorized as

$$Z(m, \mu) = \prod_k (\mu - \mu_k) \quad (15)$$

and results in the quark number density

$$n_q = \frac{1}{N N_f} \sum_k \frac{1}{\mu - \mu_k} . \quad (16)$$

Physically, we expect that the quark number density is zero below a certain nonzero critical value of  $\mu$  determined by the baryon mass. This can be achieved if the eigenvalues  $\zeta_k$  are distributed with axial symmetry in an annulus in the complex plane. Indeed, this is what has been observed numerically for QCD by Gibbs. Generally, we expect [22] that the zeros of the partition function are located on a one-dimensional manifold in the complex plane. In order to have a zero baryon density below  $\mu_c$ , a natural expectation is that the zeros are distributed homogeneously along a circle with radius  $\mu_c$ .

The resolvent is analytic in the upper complex half plane for a Hermitean Dirac operator. For nonvanishing chemical potential, the eigenvalues are scattered in the complex plane. Denoting the real and imaginary parts of the eigenvalues by  $\lambda_r$  and  $\lambda_i$ , the

eigenvalue density is characterized by a two dimensional spectral density  $\rho(\lambda_r, \lambda_i)$ . It is normalized according to

$$\int d\lambda_r d\lambda_i \rho(\lambda_r, \lambda_i) = 1 . \quad (17)$$

Using the fact that

$$\partial_{\bar{z}} \frac{1}{z} = \pi \delta^2(z) , \quad (18)$$

where the complex delta function is defined as  $\delta^2(z) = \delta(\text{Re}(z))\delta(\text{Im}(z))$ , we find

$$\rho(\lambda) = \frac{1}{\pi} \partial_{\bar{z}} G(z) \Big|_{z=\lambda} . \quad (19)$$

One of the aims of the present paper is to understand how  $G(z)$  develops nonanalyticities in the complex  $z$ -plane.

Clearly,  $G(z)$  is an analytic function of  $z$  outside the support of the spectrum of the Dirac operator. All singularities must be inside the support. In general,  $G(z)$  will have cuts in the complex plane localized within the support of the spectrum. Because of (19), the resolvent will be a function of both  $z$  and  $\bar{z}$  on the support of the spectrum.

The resolvent can be interpreted naturally in terms of a two-dimensional electrostatic problem [4]. The electric field is given by the real and imaginary parts of the resolvent and the spectral density can be interpreted as the charge density. Eq. (19) is then the two-dimensional analogue of Gauss's law:

$$\rho(\lambda_r, \lambda_i) = \frac{1}{2\pi} (\partial_x \text{Re}G(z, \bar{z}) + \partial_y \text{Im}G(z, \bar{z})) \Big|_{(x,y)=(\lambda_r, \lambda_i)} . \quad (20)$$

### 3. Simple Models

#### 3.1. Eigenvalues distributed homogeneously in the complex unit circle

To illustrate the appearance of nonanalyticities in a function that shows only an explicit dependence on  $z$ , we consider the resolvent of eigenvalues distributed uniformly inside the complex unit circle. Using the electrostatic analogy we can conclude without calculation that

$$G(z) = \theta(|z| - 1) \frac{1}{z} + \theta(1 - |z|) \bar{z} . \quad (21)$$

Let us see how we can understand this result using the average over the spectral density

$$G(z) = \int_{\text{unit circle}} d^2\lambda \frac{1}{z - \lambda} . \quad (22)$$

In polar coordinates, this integral can be written as

$$G(z) = \int_0^1 r dr \int_C \frac{du}{-i} \frac{1}{(zu - r)}, \quad (23)$$

where the contour integral is along the complex unit circle. The integrand has a simple pole at  $u = r/z$ . If  $|z| < 1$ , we obtain a contribution only for  $r < |z|$  which results in the nonanalyticity mentioned above.

### 3.2. Solution of the $2 \times 2$ matrix problem

In this section we study the resolvent for the case when  $D$  is a  $2 \times 2$  matrix. The matrix  $z - D$  can be inverted and leads to the average resolvent

$$G(z) = \frac{z}{\pi} \int_0^\infty t dt e^{-t^2} \int_0^{2\pi} d\phi \frac{1}{z^2 + t^2 - \mu^2 - i\mu t(e^{i\phi} + e^{-i\phi})}. \quad (24)$$

We write the angular integral as a contour integral along the complex unit circle

$$G(z) = \frac{z}{\pi i} \int_0^\infty t dt e^{-t^2} \int_C \frac{du}{u(z^2 + t^2 - \mu^2) - i\mu t(1 + u^2)}. \quad (25)$$

The poles of the integrand are given by the roots  $u_1$  and  $u_2$  of  $u(z^2 - t^2 + \mu^2) - i\mu t(1 + u^2) = 0$ ,

$$u_{1,2} = -i \frac{z^2 + t^2 - \mu^2}{2\mu t} \pm i \left( 1 + \frac{(z^2 + t^2 - \mu^2)^2}{4\mu^2 t^2} \right)^{1/2}, \quad (26)$$

where  $u_1$  is the root with the plus sign. Clearly, the product of the two roots is 1. Therefore nonanalyticities can only appear if the roots cross the unit circle, i.e., for  $|u_{1,2}| = 1$ . From the expression for the roots we can see that this happens if

$$\begin{aligned} \frac{z^2 + t^2 - \mu^2}{2\mu t} & \text{ is purely imaginary, and} \\ \left| \frac{z^2 + t^2 - \mu^2}{2\mu t} \right| & < 1. \end{aligned} \quad (27)$$

With the aid of the real quantity  $t_c$  defined below, these conditions are equivalent to

$$\begin{aligned} t^2 & = t_c^2 \equiv \mu^2 - \frac{1}{2}(z^2 + \bar{z}^2), \\ |\operatorname{Re} z| & \leq \mu. \end{aligned} \quad (28)$$

At the critical point the two roots interchange resulting in the resolvent

$$G(z) = 2z \int_0^\infty t e^{-t^2} \frac{1}{\mu t u_1 - u_2} - 4z\theta(\mu - |\operatorname{Re} z|) \int_0^{t_c} t e^{-t^2} \frac{1}{\mu t u_1 - u_2}. \quad (29)$$



The first term is analytic in  $z$ ; the second term, (through  $t_c$ ) depends both on  $z$  and  $\bar{z}$ . The spectral density is then given by

$$\rho(\lambda_r, \lambda_i) = \frac{1}{\pi} \partial_{\bar{z}} G(z) \Big|_{z=\lambda_r+i\lambda_i} = \theta(\mu - |\lambda_r|) \frac{1}{\pi} \frac{(\lambda_r^2 + \lambda_i^2) e^{-(\mu^2 - \lambda_r^2 + \lambda_i^2)}}{\sqrt{\mu^2 - \lambda_r^2} \sqrt{\mu^2 + \lambda_i^2}} . \quad (30)$$

It is straightforward to repeat this calculation for the unquenched case. The condensate can be obtained from the partition function which, for one flavor, is given by

$$Z(m) = \int_0^\infty t dt e^{-t^2} \int_0^{2\pi} d\phi \det(m - D) , \quad (31)$$

where

$$\det(m - D) = m^2 + t^2 - \mu^2 - i\mu t(e^{i\phi} + e^{-i\phi}) . \quad (32)$$

The integrals are elementary resulting in the partition function

$$Z(m) = \pi(m^2 - \mu^2 + 1) . \quad (33)$$

The corresponding chiral condensate is given by

$$\Xi(m) = \frac{2m}{m^2 - \mu^2 + 1} . \quad (34)$$

For one flavor the resolvent is defined by

$$G^{N_f=1}(z) = \frac{1}{Z(m)} \int_0^\infty t dt e^{-t^2} \int_0^{2\pi} d\phi \frac{1}{2} \text{Tr} \frac{1}{z - D} \det(m - D) , \quad (35)$$

which can be written as

$$G^{N_f=1}(z) = \frac{1}{m^2 - \mu^2 + 1} \left[ z + (m^2 - z^2) G^{N_f=0}(z) \right] . \quad (36)$$

We see that nonanalyticities are absent for  $z = m$ . This was to be expected because the singularities of the resolvent are cancelled by the zeros of the determinant. A similar cancellation takes place in the Gibbs model to be discussed in the next section.

#### 4. The resolvent in the Gibbs model

In this section we analyze the resolvent of the model proposed by Gibbs [10]. In this model the Dirac operator is defined by

$$D_{kl}^G + m\delta_{k,l} = -\delta_{k,l+1} e^{-i\theta - \mu} + \delta_{k,l-1} e^{i\theta + \mu} + m\delta_{k,l} , \quad (37)$$

where the indices are modulo  $N$ . Anti-periodic boundary conditions result in an extra minus sign for the matrix elements  $D_{1n}^G$  and  $D_{n1}^G$ . The partition function is obtained by averaging over  $\theta$ ,

$$Z = \int d\theta \det^{N_f}(D^G + m) . \quad (38)$$

The eigenvalues of  $D^G$  are given by

$$\lambda_k = e^{\frac{2\pi i(k+1/2)}{N} + i\theta + \mu} - e^{-\frac{2\pi i(k+1/2)}{N} - i\theta - \mu} , \quad (39)$$

where  $k = 1, \dots, N$ . Geometrically they fall on an ellipse in the complex plane with semiaxis  $e^\mu - e^{-\mu}$  in the real direction and semiaxis  $e^\mu + e^{-\mu}$  in the imaginary direction. The fermion determinant follows from the solution of a recursion relation

$$\det D^G = e^{-N(i\theta + \mu)} + e^{-N(i\theta + \mu)} + \lambda_2(m)^N + \lambda_1(m)^N , \quad (40)$$

where

$$\lambda_{1,2}(z) = \frac{z}{2} \mp \sqrt{1 + \frac{z^2}{4}} . \quad (41)$$

The resolvent, defined by

$$G(z) = \frac{1}{Z} \int d\theta \det^{N_f} D^G \frac{1}{N} \sum_k \frac{1}{z - \lambda_k} , \quad (42)$$

will be evaluated for  $N_f = 0$  and  $N_f = 1$ . (Here,  $Z$  is the partition function)

The integral over  $\theta$  can be performed conveniently by contour integration. The phase of the eigenvalues and the chemical potential can be absorbed in  $\theta$  resulting in an integral over a circle in the complex plane with radius  $e^\mu$ . For  $N_f = 1$  we find

$$\begin{aligned} G(z) = & \theta(|\lambda_2(z)| - e^\mu) \frac{1}{\lambda_2(z) - \lambda_1(z)} \left( 1 - \frac{2\lambda_1^N(z)}{\lambda_1^N(m) + \lambda_2^N(m)} \right) \\ & + \theta(e^\mu - |\lambda_2(z)|) \frac{1}{\lambda_2(z) - \lambda_1(z)} \frac{\lambda_2^N(z) - \lambda_1^N(z)}{\lambda_1^N(m) + \lambda_2^N(m)} . \end{aligned} \quad (43)$$

This is valid with the convention that  $|\lambda_2(z)| \geq |\lambda_1(z)|$ .

Note that  $|\lambda_1| = |\lambda_2| = 1$  when  $z = is$  is purely imaginary and  $s < 2$  and positive. For  $s > 2$  our convention reads

$$\begin{aligned} \lambda_1 &= \frac{is}{2} - \frac{i}{2} \sqrt{s^2 - 4} , \\ \lambda_2 &= \frac{is}{2} + \frac{i}{2} \sqrt{s^2 - 4} . \end{aligned} \quad (44)$$

The condition  $|\lambda_2(z)| = e^\mu$  can be rewritten as

$$\begin{aligned} z &= e^\mu - e^{-\mu} && \text{for } z \text{ real} \\ z &= e^\mu + e^{-\mu} && \text{for } z \text{ imaginary .} \end{aligned} \tag{45}$$

This implies that  $z$  coincides with the modulus of the eigenvalues on the real and imaginary axis, respectively.

In the quenched approximation, we obtain

$$G(z) = \theta(|\lambda_2(z)| - e^\mu) \frac{1}{\lambda_2(z) - \lambda_1(z)} , \tag{46}$$

which is valid for the same convention,  $|\lambda_2(z)| \geq |\lambda_1(z)|$ .

We find that quenched and unquenched results agree in the thermodynamic limit if  $|z|$  is larger than the modulus of any of the eigenvalues. For  $N \rightarrow \infty$  and real  $z = r$  inside the ellipse of eigenvalues, the unquenched resolvent diverges for  $m < r < e^\mu - e^{-\mu}$  and is zero for  $r < m$ . The quenched result is zero. Quenching works if  $m$  is outside the ellipse of eigenvalues. For imaginary  $z = is$ , quenching succeeds for  $s < \sqrt{m^2 + 4}$  but fails in the region  $\sqrt{m^2 + 4} < s < e^\mu + e^{-\mu}$ . For  $m > e^\mu - e^{-\mu}$  quenching works for all values of  $s$ .

In Fig. 1 we illustrate the above quenched and unquenched results for the case  $m = 0$ ,  $\mu = 0.2$  and  $N = 8$ . We show the resolvent for  $z$  real (left) and  $z$  imaginary (right). This figure clearly shows the region where quenching fails.

It is instructive to consider the thermodynamic limit of  $G(z)$  for  $z \rightarrow m$  in the unquenched case. We expect that this limit exists because the singularities of the resolvent are cancelled by the zeros of the determinant. Indeed, for  $z \rightarrow m$  we find

$$G(z) = \theta(|\lambda_2(z)| - e^\mu) \frac{1}{\lambda_2(m) - \lambda_1(m)} + \theta(e^\mu - |\lambda_2(z)|) \frac{1}{\lambda_2(m) - \lambda_1(m)} \left( \frac{\lambda_2(z)}{\lambda_2(m)} \right)^N , \tag{47}$$

which is finite for  $z = m$ . The result for  $G(z)$  is independent of  $z$  and identical to  $\frac{1}{N} \partial_m \log Z$  in the thermodynamic limit.

## 5. Random matrix model

In this section we study the partition function

$$Z(m, \mu) = \int DW P(W) \det^{N_f} \begin{pmatrix} m & iW + \mu \\ iW^\dagger + \mu & m \end{pmatrix} , \tag{48}$$

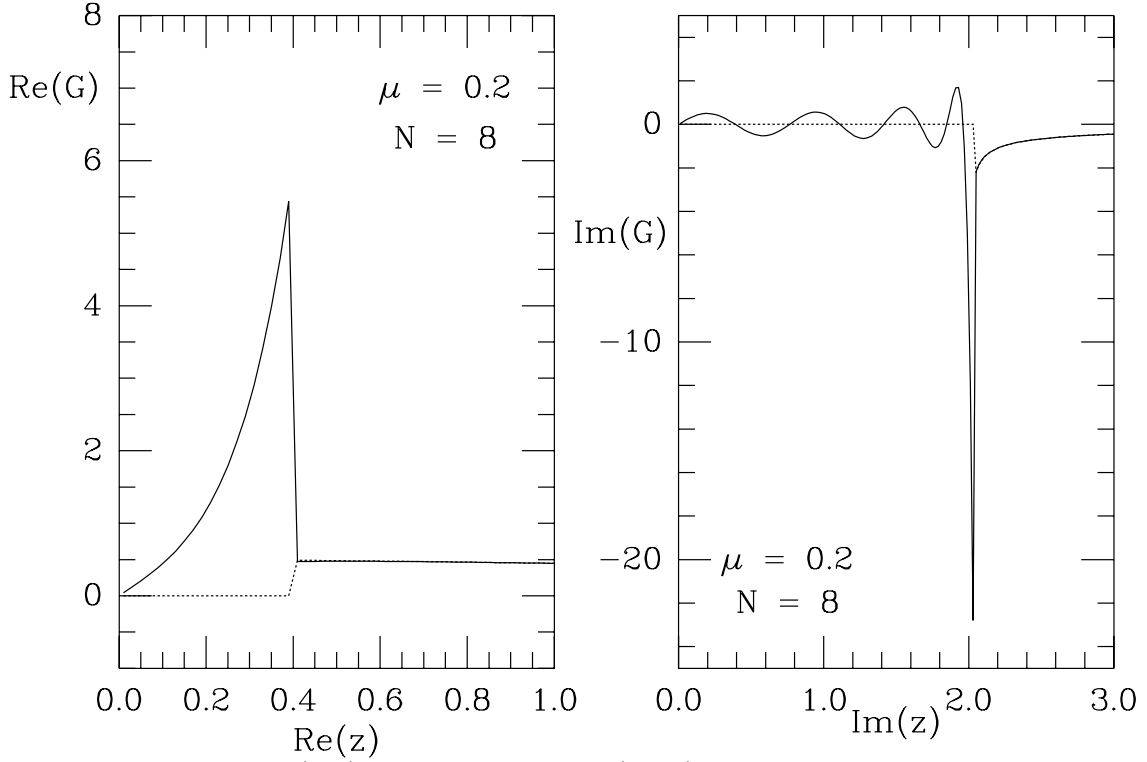


Fig. 1. The real (left) and the imaginary (right) parts of the resolvent in the Gibbs model on the real and imaginary axis, respectively. Results are shown for  $\mu = 0.2$  and  $n = 8$ . The full curve represents the result for one flavor and the dashed curve for zero flavors.

where  $W$  is an arbitrary complex  $n \times n$  matrix and  $DW$  the Haar measure. The probability distribution  $P(W)$  is given by

$$P(W) = \exp(-n\Sigma^2 \text{Tr}WW^\dagger) . \quad (49)$$

The fermion determinant in (48) can be written as a Grassmann integral.

$$Z(m, \mu) = \int \mathcal{D}W \mathcal{D}\psi^* \mathcal{D}\psi \exp \left[ -i \sum_{k=1}^{N_f} \psi^{k*} \begin{pmatrix} m & iW + \mu \\ iW^\dagger + \mu & m \end{pmatrix} \psi^k \right] \exp[-n\Sigma^2 \text{Tr}WW^\dagger] . \quad (50)$$

This enables us to perform the  $W$  integration

$$Z(m, \mu) = \int \mathcal{D}\psi^* \mathcal{D}\psi \exp \left[ -\frac{1}{n\Sigma^2} \psi_{Lk}^{f*} \psi_{Ri}^f \psi_{Ri}^{g*} \psi_{Lk}^g + m \left( \psi_{Ri}^{f*} \psi_{Ri}^f + \psi_{Lk}^{f*} \psi_{Lk}^g \right) + \mu \left( \psi_{Ri}^{f*} \psi_{Li}^f + \psi_{Lk}^{f*} \psi_{Rk}^f \right) \right] . \quad (51)$$

The four-fermion terms can be written as the difference of two squares. Each square can be linearized by a Hubbard-Stratonovitch transformation according to

$$\exp(-AQ^2) \sim \int d\sigma \exp\left(-\frac{\sigma^2}{4A} - iQ\sigma\right) . \quad (52)$$

Thus, the fermionic integrals can be performed, and the partition function can be written as a single integral over the complex  $N_f \times N_f$  matrix,  $\sigma$ ,

$$Z(m, \mu) = \int \mathcal{D}\sigma \exp[-n\Sigma^2 \text{Tr}\sigma\sigma^\dagger] \det^n \begin{pmatrix} \sigma + m & \mu \\ \mu & \sigma^\dagger + m \end{pmatrix} . \quad (53)$$

The condensate is given by

$$\langle \bar{q}q \rangle = \frac{1}{2nN_f} \partial_m \log Z \equiv G(m) . \quad (54)$$

For  $n \rightarrow \infty$ , it can be evaluated with the aid of a saddle point approximation. The saddle point equations are given by

$$-\Sigma^2\sigma + (\sigma + m) \left( (\sigma^\dagger + m)(\sigma + m) - \mu^2 \right)^{-1} = 0 , \quad (55)$$

and an equation with  $\sigma$  and  $\sigma^\dagger$  interchanged. The solutions are proportional to the identity with diagonal elements given (for  $\Sigma = 1$ ) by

$$\begin{aligned} \sigma^* &= \sigma, \\ \sigma(m + \sigma)^2 - \mu^2\sigma &= m + \sigma . \end{aligned} \quad (56)$$

This equation was first derived [23] for the finite temperature version of the model [23–25]. (obtained from (53) by the substitution  $\mu \rightarrow -iT$ ). The condensate is then given by

$$\langle \bar{q}q \rangle = G(m) = \sigma . \quad (57)$$

The quark number density defined in (13) can be related to  $\sigma$ ,

$$n_q = \frac{-\mu\sigma}{\sigma + m} \quad (58)$$

For  $m = 0$  it is possible to have a discontinuity in  $\langle \bar{q}q \rangle$  but not in  $n_q$ . Notice that in the restored phase with  $\sigma = 0$  this expression has to be treated with care. In fact, from the saddle point equation we obtain  $n_q = 1/\mu$  for  $\sigma = 0$ , and  $n_q = -\mu$  for  $\sigma \neq 0$ . In general,

we expect that a discontinuity in the chiral condensate is accompanied by a discontinuity in the quark number density.

Two solutions of (56) coincide if the discriminant of the cubic equation,

$$D_3 = \frac{1}{27} \left( m^4 \mu^2 - m^2 \left( 2\mu^4 - 5\mu^2 - \frac{1}{4} \right) + (1 + \mu^2)^3 \right) , \quad (59)$$

vanishes.

In the finite temperature version of the present model [23], we evaluated the average resolvent for  $z$  on the positive real axis and obtained the resolvent for  $\text{Re}(z) > 0$  through analytical continuation. This is justified because the resolvent is analytic in this part of the complex plane. The average resolvent was calculated with two methods [26]: (i) the super-symmetric method, and (ii) a self-consistent equation for the resolvent for  $n \rightarrow \infty$ . The first method is much more intricate with regards to analyticity and convergence than the second. For the moment, we discuss only the second method. The self-consistent equation was obtained from a series expansion of the resolvent  $G(z)$  in powers of  $z^{-1}$ . This is justified if  $|z|$  is larger than the largest eigenvalue. In our present model with a chemical potential, this is still true. It should also be clear that the resolvent is analytic in  $z$  everywhere outside of the support of the eigenvalue spectrum of the Dirac operator. In other words, the singularities of  $G(z)$  should be inside the support of the spectrum of the Dirac operator. However, for  $z$  inside the domain of eigenvalues, the series expansion is not justified. Indeed, the resolvent in this region is not given by the cubic equation (56), as was shown by Stephanov [12]. After replacing  $T \rightarrow i\mu$  and making an appropriate rotation in the complex plane (the Dirac operator in [23,26] differs by a factor  $i$  from the Dirac operator in the present work), the self-consistent cubic equation in [23,26] is seen to be identical to the cubic equation (56).

### 5.1. Unquenched partition function

In this section we analyze the partition function (53) for one flavor. In units where  $\Sigma = 1$ , it is given by

$$Z(m, \mu) = \int d\sigma d\sigma^* e^{-n\sigma^2} (\sigma\sigma^* + m(\sigma + \sigma^*) + m^2 - \mu^2)^n . \quad (60)$$

After shifting the real part of  $\sigma$  by  $m$ , we use polar coordinates as new integration variables. If we notice that the angular integral represents a modified Bessel function, the

partition function can be written as

$$Z(m, \mu) = \pi e^{-nm^2} \int_0^\infty du (u - \mu^2)^n I_0(2mn\sqrt{u}) e^{-nu} . \quad (61)$$

In the thermodynamic limit, this partition function can be evaluated by a saddle point approximation. Using the asymptotic form of  $I_0(z) \sim e^z / \sqrt{2\pi z}$ , the saddle point equation reads

$$\frac{1}{u - \mu^2} = 1 - \frac{m}{\sqrt{u}} . \quad (62)$$

A phase transition takes place at the points where  $|Z_{u=u_b}| = |Z_{u=u_r}|$ , with  $u_b$  and  $u_r$  two solutions of the saddle-point equation (62). This condition can be rewritten as

$$|(u_b - \mu^2)e^{2m\sqrt{u_b} - u_b}| = |(\mu^2 - u_r)e^{2m\sqrt{u_r} - u_r}| . \quad (63)$$

The selection of the dominant saddle-points requires a detailed analysis of the partition function (see below). This will lead to some restrictions on the range of  $\mu$  and  $m$  determined by the zeros of the discriminant (59). Below we will show that (63) determines the location of the zeros of the partition function. The additional limitations on the range of the critical values of  $m$  and  $\mu$  immediately follow from such analysis.

In general, the solution of these equations is cumbersome. However, for  $m \rightarrow 0$  we find that  $u_r = 0$  and  $u_b = 1 + \mu^2$ . This leads to the critical curve

$$\text{Re} \left[ 1 + \mu^2 + \log \mu^2 \right] = 0 . \quad (64)$$

For real  $\mu$ , the solution is given by  $\mu_c = 0.527\dots$ ; for purely imaginary  $\mu$ , we find  $\mu_c = i$ . Moreover, from a detailed saddle-point analysis it can be shown that the partition function only shows a discontinuity for those values of  $\mu$  that in addition to (64) also satisfy  $|\mu| < 1$ .

We wish to analyze the zeros of the partition function (60) in the complex  $m$  plane and the complex  $\mu$  plane. In order to obtain the polynomial in  $m$  and  $\mu$ , we expand the binomial in (61) and perform the integration over  $u$ . The result can be expressed using confluent hypergeometric functions

$$Z(m, \mu) = \frac{\pi n! e^{-nm^2}}{n^{n+1}} \sum_{k=0}^n \frac{(-\mu^2 n)^k}{k!} {}_1F_1((n - k + 1), 1, m^2 n) . \quad (65)$$

According to the Kummer identity we have

$$e^{-nm^2} {}_1F_1((n - k + 1), 1, m^2 n) = {}_1F_1(-(n - k), 1, -m^2 n) \quad (66)$$

which is a polynomial of order  $n - k$  in  $-m^2n$ . From the standard representation of this Kummer function we obtain

$$Z(m, \mu) = \frac{\pi n!}{n^{n+1}} \sum_{k=0}^n \sum_{l=0}^{n-k} \frac{1}{l!k!} \binom{n-k}{l} (-\mu^2n)^k (m^2n)^l. \quad (67)$$

Although the sums in (67) are finite, the alternating nature of the series and the degree of cancellation make numerical evaluation difficult.

For real  $\mu$  the phase structure of the partition function (61) can be clarified by the decomposition

$$Z(m, \mu) = Z^{\text{broken}}(m, \mu) + Z^{\text{restored}}(m, \mu), \quad (68)$$

where

$$\begin{aligned} Z^{\text{broken}}(m, \mu) &= \pi e^{-nm^2} \int_{\mu^2}^{\infty} du (u - \mu^2)^n I_0(2mn\sqrt{u}) e^{-nu} \\ Z^{\text{restored}}(m, \mu) &= \pi e^{-nm^2} \int_0^{\mu^2} du (\mu^2 - u)^n I_0(2mn\sqrt{u}) e^{-nu}. \end{aligned} \quad (69)$$

From a graphical representation of both sides of the saddle point equation (62) it is clear that one solution is in the interval  $[0, \mu^2]$ , which we call  $u_r$ , another is in the interval  $[\mu^2, \infty)$ , which we will call  $u_b$  and another has  $\sqrt{u} < 0$ . A phase transition takes place at the point where  $|Z_{u=u_b}| = |Z_{u=u_r}|$ . For  $m = 0$  the thermodynamic limit of the partition function is then given by

$$Z(m = 0, \mu) = \theta(\mu_c - \mu) \frac{\pi^{3/2}}{\sqrt{n}} e^{-n(1+\mu^2)} + \theta(\mu - \mu_c) \frac{\pi^{3/2}}{\sqrt{n}} \mu^{2n}. \quad (70)$$

The partition function can be calculated in a much more effective way if we rewrite it as a sum of positive definite terms. For the broken part, we expand  $I_0$  in a power series and change integration variables according to  $u \rightarrow \mu^2(1 + u)$ . The integrals can be performed following expansion of the binomial and result in

$$Z^{\text{broken}}(m, \mu) = \frac{\pi e^{-n(m^2+\mu^2)}}{n^{n+1}} \sum_{l=0}^{\infty} \sum_{s=0}^l \frac{(n+s)!}{l!s!(l-s)!} (m^2n)^l (\mu^2n)^{l-s}. \quad (71)$$

For the restored part, we also expand the modified Bessel function but change integration variables according to  $u \rightarrow \mu^2(1 - u)$ . The integral of each term in the expansion of  $\exp(n\mu^2u)$  is a beta function. Collecting powers and factorials we obtain

$$Z^{\text{restored}}(m, \mu) = \pi \mu^{2(n+1)} e^{-n(m^2+\mu^2)} \sum_{l=0}^{\infty} \sum_{s=0}^{\infty} \frac{(n+s)!}{l!s!(n+s+l+1)!} (m^2n)^l (\mu^2n)^{l+s}. \quad (72)$$

This expression has been used for a numerical study of the partition function.



## 5.2. Yang-Lee zeros

In this section we evaluate the Yang-Lee zeros of the partition function (67) and show that their location is consistent with a saddle-point analysis of the partition function. First, we consider the partition function as a polynomial in  $m$ . Results for  $\mu = 0$ ,  $\mu = 0.5$ , and  $\mu = 0.6$  are shown in the left column of Fig. 2. We have calculated the zeros for different values of  $n$ , e.g.,  $n = 48$ ,  $n = 96$ , and  $n = 192$ . The results for  $n = 192$  are represented by the points in the figure. Of course, the exact location of the zeros is extremely sensitive to numerical round-off errors. Thus, the present results were obtained with the help of a multi-precision package [28]. Typically, we performed our computations with 100-500 digits accuracy.

The zeros fall on a curve and are regularly spaced<sup>1</sup>. It is clear from the saddle point analysis of the partition function that a single condition is imposed on the the complex variable  $m$  by the condition that the free energy of two different saddle point solutions coincides. This explains the fact that, in the thermodynamic limit, the zeros are located on a curve in the complex plane. (A similar argument has been given for the Ising model [22].) If we increase the order of the polynomial by a factor of 2, we find that half of the zeros are close to those of the lower-order polynomial. The other half of the zeros are roughly mid-way between adjacent zeros of the lower-order polynomial. This leads us to the conclusion that the zeros become dense and lead to a cut in the complex  $m$  plane in the thermodynamic limit.

The stars in Fig. 2 represent the points at which the discriminant (59) of the cubic saddle point equation vanishes. These points coincide with the endpoints of the line of zeros. In the right column of Fig. 2 we show the curves in the complex  $m$ -plane across which there is a transition in the dominant solution of the third-order equation (56). The analytical result for this curve is given in (63). A schematic picture of the latter was also shown in [29].

In the left column of Fig. 3, we show the zeros of the partition function in the complex  $\mu$  plane for  $n=192$  and masses  $m = 0$ ,  $m = 0.3$ , and  $m = 1.0$ . We have evaluated the zeros

---

<sup>1</sup>If the numerical accuracy is not sufficient, one typically observes that the line of zeros ends in a circle.

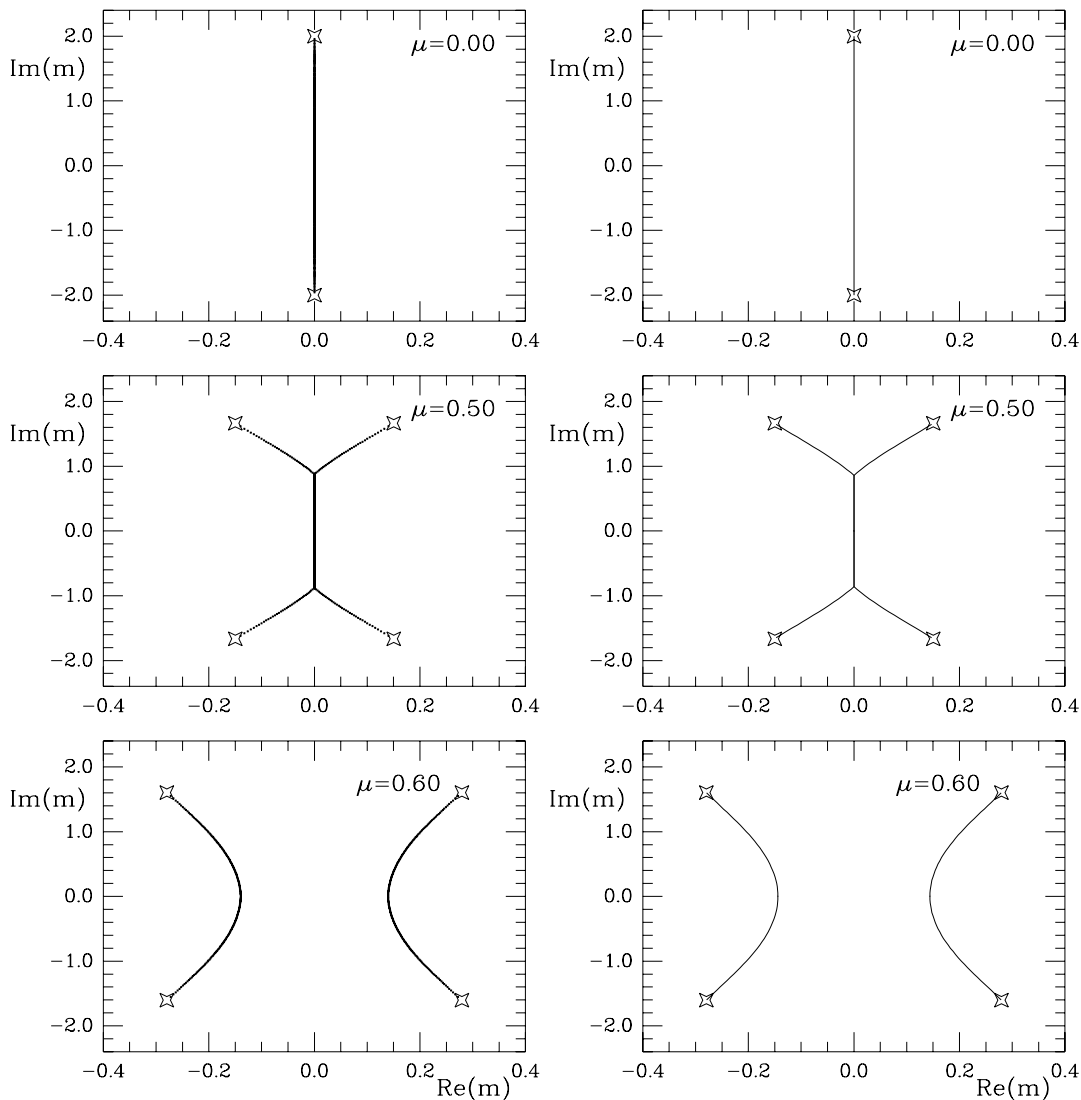


Fig. 2. The zeros of the partition function in the complex  $m$  plane (left), and the curves where the mean field result for the resolvent shows a discontinuity (right). Results are given for  $\mu = 0$  (upper),  $\mu = 0.50$  (middle) and  $\mu = 0.60$  (lower) for  $n = 192$ . Zeros of the discriminant of the cubic equation (56) are denoted by stars.

for  $n = 48$  and  $n = 96$ . Here, too, all calculations were performed with 100-500 digits accuracy. The zeros are regularly spaced, and their density increases homogeneously with  $n$ . In the thermodynamic limit, we therefore expect that they join into a cut. In all cases, the line of zeros terminates at a zero of the discriminant (59), which is denoted by a star. In right column of Fig. 3, we show the curve across which the saddle point result for the chiral condensate shows a discontinuity. Below (58) it was argued that this will lead to a discontinuity in the quark number density as well. Notice that for  $m = 0$  the

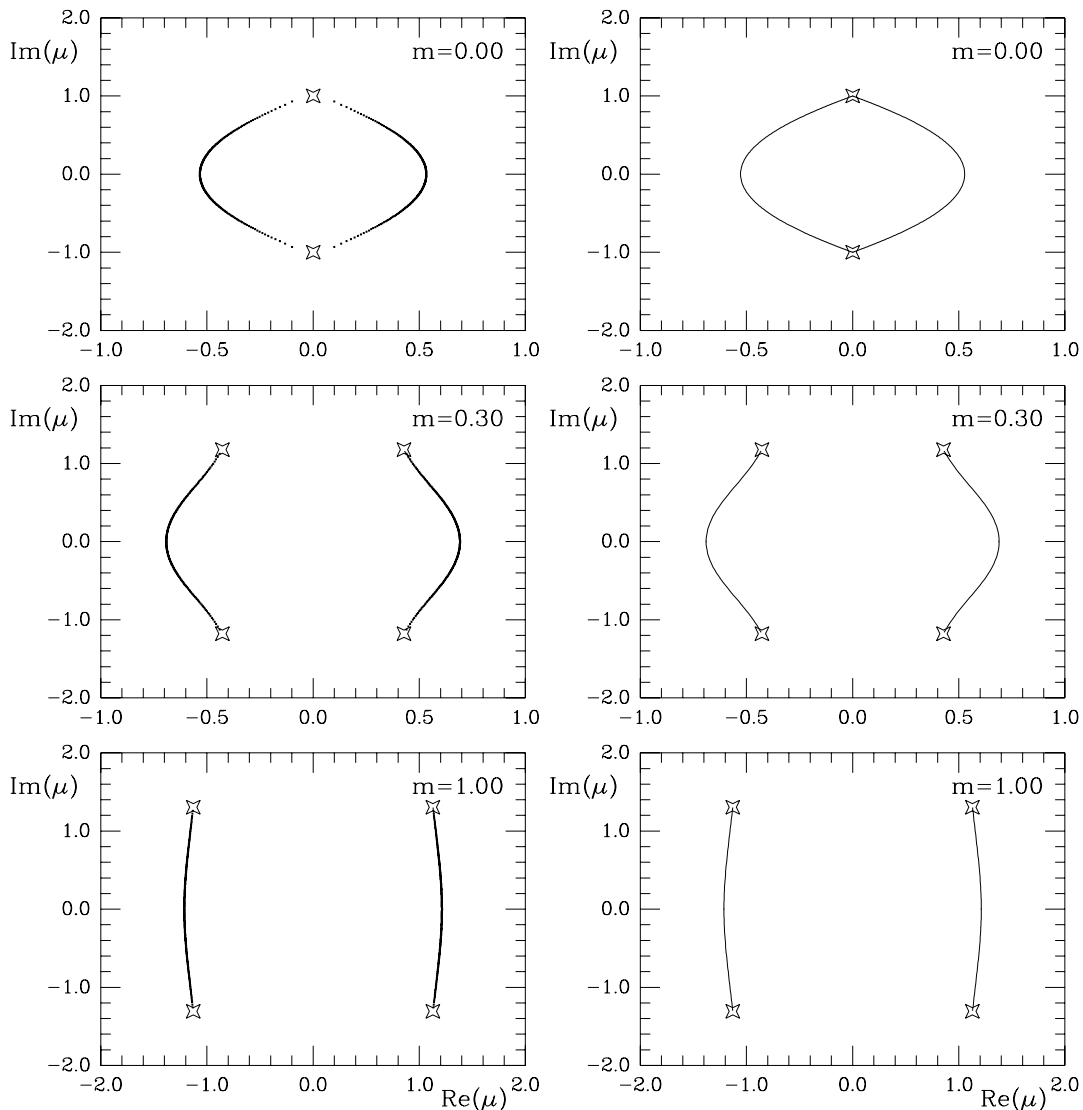


Fig. 3. The zeros of the partition function in the complex  $\mu$  plane (left) and the location of points where the mean field result for the chiral condensate shows a discontinuity (right). Results are given for for  $m = 0$  (upper),  $m = 0.30$  (middle), and  $m = 1.0$  (lower) for  $n = 192$ . The stars represent zeros of the discriminant of the cubic equation (56). Note that the scale on the  $x$ -axis of the lower figure is different.

chiral condensate jumps from a finite value to zero. The analytical result follows from the transcendental equation (63) For  $m = 0$ , chiral symmetry is broken in the region enclosed by this curve and is restored outside. In this case, the density of zeros approaches zero near  $\mu = i$ . This is not surprising since, at this point, the phase transition changes from first to second order.

## 6. Quark number density

In this section we study the effect of the fermion determinant and eigenvalue correlations on the quark number density defined in (13). In the quenched approximation the quark number density is given by

$$n_q = \frac{1}{N} \text{Tr} \left( \begin{array}{cc} iW + \mu & m \\ m & iW^\dagger + \mu \end{array} \right)^{-1}, \quad (73)$$

where  $W$  is distributed according to (3). For  $m$  equal to zero, the quark number density follows from the spectral density of the ensemble of matrices

$$\left( \begin{array}{cc} iW & 0 \\ 0 & iW^\dagger \end{array} \right). \quad (74)$$

This ensemble was analyzed by Ginibre [27]. An arbitrary complex matrix can be diagonalized by a similarity transformation

$$W = X \Lambda X^{-1}, \quad (75)$$

where  $\Lambda$  is a complex diagonal matrix. In this case, the Gaussian probability distribution depends both on  $\Lambda$  and  $X$ . Thus, the problem of determining the joint probability distribution of the eigenvalues is not solved by simply choosing the eigenvalues and eigenvectors as new integration variables. However, using a remarkable precursor of an Itzykson-Zuber integral, Ginibre was able to solve the problem analytically. In the thermodynamic limit, the eigenvalues of  $W$  (and therefore of  $W^\dagger$ ,  $iW$  and  $iW^\dagger$ ) are distributed uniformly in the complex unit circle. As we will show below, results in a nonzero quark number density for arbitrary small  $\mu$ . In terms of the eigenvalues, the baryon number density is given by

$$n_q = \frac{1}{N} \sum_k \left[ \frac{1}{\lambda_k + \mu} + \frac{1}{\lambda_k^* + \mu} \right]. \quad (76)$$

For eigenvalues distributed uniformly inside the unit circle, the baryon number density can be evaluated in the same way as the chiral condensate in section 2. The result is:

$$n_q = \theta(1 - \mu)\mu + \theta(\mu - 1)\frac{1}{\mu}. \quad (77)$$

For the unquenched case, the baryon number density in the broken phase is quite different with

$$n_q = \theta(\mu_c - \mu)(-\mu) + \theta(\mu - \mu_c)\frac{1}{\mu}. \quad (78)$$

Finally, we wish to stress that the correlations of the eigenvalues play an important role in establishing the result (78). For uncorrelated eigenvalues distributed homogeneously inside the complex unit circle, the unquenched partition function factorizes into

$$\begin{aligned} Z(\mu) &= \left[ \frac{1}{\pi} \int_D d^2\lambda (\mu^2 - |\lambda|^2 + i\mu(\lambda + \lambda^*)) \right]^n \\ &= \left( \mu^2 - \frac{1}{2} \right)^n . \end{aligned} \quad (79)$$

The quark number density, which is then given by

$$n_q = \frac{\mu}{\mu^2 - \frac{1}{2}} , \quad (80)$$

shows some of the characteristic features of the unquenched result, including a discontinuity at a critical value of  $\mu$ . In terms of the joint eigenvalue distribution of the random matrix ensemble (1), the partition function is given by

$$Z(\mu) = \frac{1}{\mathcal{N}} \int \prod_k d\lambda_k d\lambda_k^* \prod_k [\mu^2 - |\lambda_k|^2 + i\mu(\lambda_k + \lambda_k^*)] \prod_{k<l} |\lambda_k - \lambda_l|^2 \exp(-|\lambda|^2) , \quad (81)$$

where  $\mathcal{N}$  is a normalization constant. The correlations between the eigenvalues which are mainly induced by the Vandermonde determinant in (81) leads to a partition function that is completely different from (81). (In the thermodynamic limit (81) reduces to (70)). In particular, the zeros of (81) are  $n$ -fold degenerate, whereas the zeros of (60) are located on a closed curve as shown in Fig. 3.

It is equally straightforward to obtain the result with the determinant replaced by its absolute value. Then,

$$\begin{aligned} Z(\mu) &= \left[ \frac{1}{\pi} \int_D d^2\lambda (\mu^2 + |\lambda|^2 + i\mu(\lambda + \lambda^*)) \right]^n \\ &= \left( \mu^2 + \frac{1}{2} \right)^n . \end{aligned} \quad (82)$$

The quark number density, now given by

$$n_q = \frac{\mu}{\mu^2 + \frac{1}{2}} , \quad (83)$$

is much closer to the quenched result.

We conclude that quenching has a major effect on the quark number density. We have also found that correlations between the eigenvalues play an important role in establishing the  $\mu$ -dependence of the partition function.

## 7. Numerical results for the unquenched resolvent

In section 4 we demonstrated that, for  $z$  less than some critical value, the resolvent of the unquenched Gibbs model diverges in the thermodynamic limit. We note that this model is special in the sense that its eigenvalues fall on a one-dimensional manifold in the complex plane (i.e., an ellipse), which is not the case in lattice QCD simulations [4]. In this section we study the model (1), which has a genuinely two-dimensional spectral distribution. Unfortunately, we have not been able to treat the unquenched case analytically. However, it can be attacked numerically by brute force, i.e., the fermion determinant is not included in the measure but rather in the observable. Results for  $G(z)$  on the real and imaginary axes are shown in Figs. 4, 5 and 6. In Fig. 4 we show the real part of the resolvent for  $\mu = 0.2$  and  $n = 24$  (left) and  $n = 48$  (right). The mass in the determinant is equal to zero. The full line represents unquenched results for the resolvent. The analytical quenched results are represented by the dotted curves. The almost horizontal dotted curve shows the solution given by the cubic equation (56). The dotted curve through zero is the Stephanov solution [12] which is given in general by

$$G(z = x + iy) = \frac{1}{2} \frac{x}{\mu^2 - x^2} - x - \frac{iy}{2} . \quad (84)$$

Up to corrections of order  $1/n$  the quenched numerical result (dashed curve) is in agreement with the Stephanov solution inside the domain of eigenvalues ( $|x| < 0.0732$  for  $\mu = 0.2$  and  $|x| < 0.1504$  for  $\mu = 0.3$ ) and follows the solution of the cubic equation outside this domain. In this region the unquenched resolvent agrees with the quenched resolvent up to corrections of order  $1/n$ . The most dramatic result of this calculation is that the real part of the resolvent seems to diverge for  $z$  inside the domain of eigenvalues. This is in complete agreement with the observation made for the Gibbs model. The slope near zero is strictly proportional to  $n$ . This can be understood analytically from the absence of eigenvalues in this region. Therefore, the resolvent can be expanded as

$$G(z) = z \frac{1}{2n} \sum_k \frac{-1}{\lambda_k^2} + O(z^3) . \quad (85)$$

The inverse moment of the eigenvalues follows immediately from the proper unquenched partition function (60)

$$\frac{1}{2} \sum_k \frac{-1}{\lambda_k^2} = \partial_{m^2} \log Z = n^2(1 + \mu^2) \quad (86)$$

resulting in

$$G(z) = zn(1 + \mu^2) + O(z^3) , \quad (87)$$

which is in perfect agreement with the numerical results.

Results for the real part of the resolvent for  $n = 24$  and  $\mu = 0.3$  are shown in Fig. 6. We find that the maximum increases strongly with  $\mu$ . This should be contrasted with the same model at finite temperature where the average resolvent is flavor independent.

The imaginary part of the resolvent is shown in Figs.5 and 6 as a function of the imaginary part of  $z$ . The fluctuations of the unquenched result are much stronger in this case. Remarkably, the unquenched result seems to agree with the quenched result (dotted curve) for all real  $z$ . The area of the peak near zero is proportional to  $1/n$  which suggests that this is a finite size effect. Notice that inside the domain of eigenvalues the analytical result (i.e., the Stephanov solution) does not depend on  $\mu$ . Only the point where the two solutions intersect is  $\mu$ -dependent.

The results for  $n = 48$  and  $\mu = 0.2$  were obtained by averaging over one million matrices. Results for  $\mu = 0.3$  and  $n = 24$  required as many as three million matrices. The difficulties in simulating the partition function becomes clearer if we consider the expectation value of the fermion determinant which is given by the partition function for one flavor. Let us write out explicitly the determinant in the definition (4) of the unquenched resolvent

$$G(z) \equiv \frac{1}{N} \left\langle \text{Tr} \left( \frac{1}{z - D} \right) \right\rangle \equiv \frac{\langle \langle \det^{N_f}(m - D) \text{Tr} \left( \frac{1}{z - D} \right) \rangle \rangle}{\langle \langle \det^{N_f}(m - D) \rangle \rangle} , \quad (88)$$

where  $\langle \langle \dots \rangle \rangle$  stands for averaging without including the determinant in the weight. The normalization is just the unquenched partition function. For one flavor, it was evaluated in (66). In the broken phase it is given by

$$Z(m = 0, \mu) = \frac{\pi^{3/2}}{\sqrt{n}} e^{-n(1+\mu^2)} \quad (89)$$

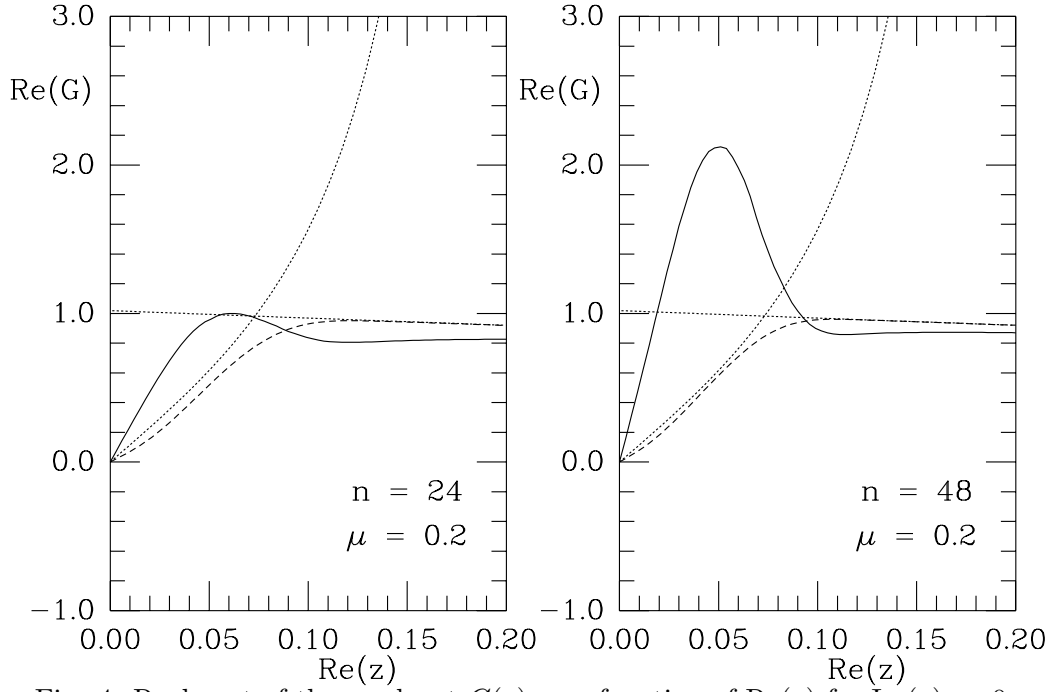


Fig. 4. Real part of the resolvent  $G(z)$  as a function of  $\text{Re}(z)$  for  $\text{Im}(z) = 0$ .

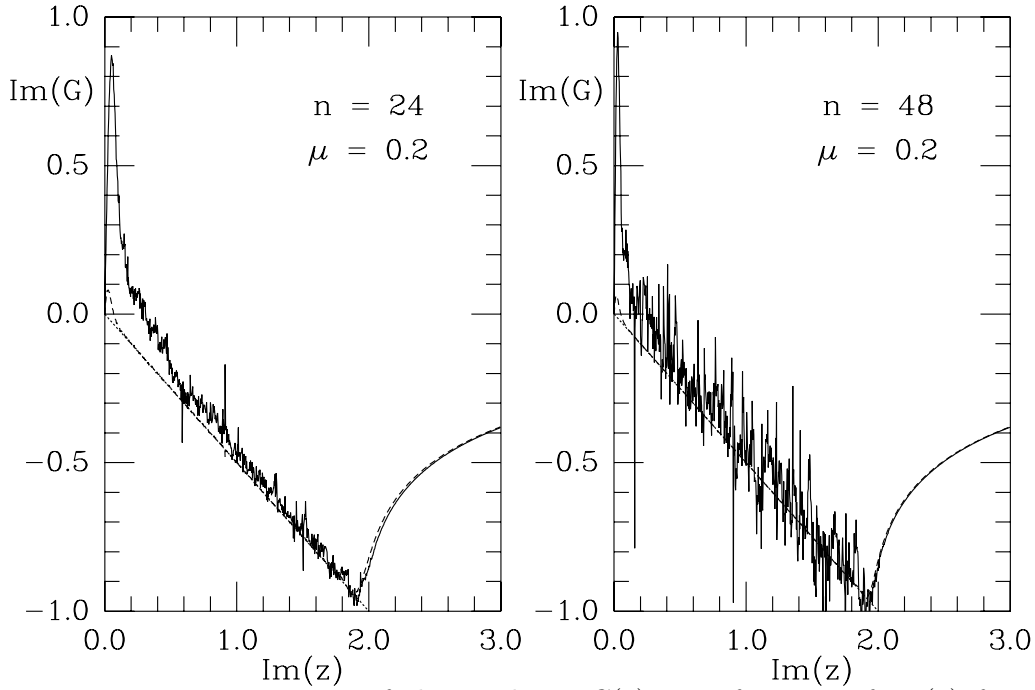


Fig. 5. Imaginary part of the resolvent  $G(z)$  as a function of  $\text{Im}(z)$  for  $\text{Re}(z) = 0$ .

This exponential suppression makes it prohibitively difficult to calculate the unquenched resolvent via a Monte Carlo method. Indeed, we find that the convergence of numerical



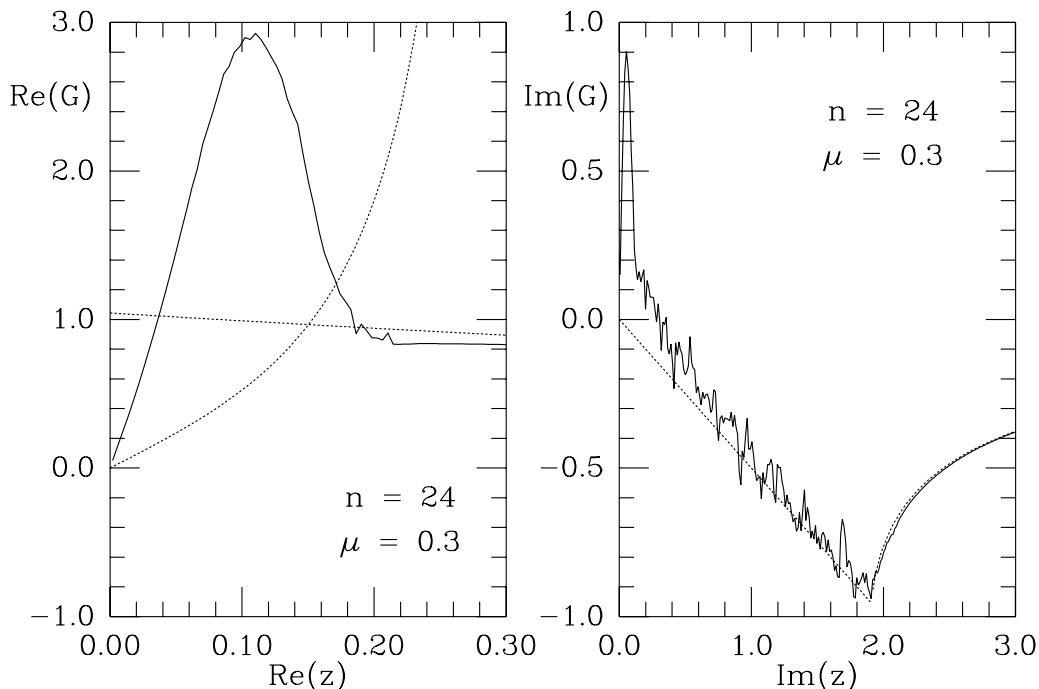


Fig. 6. Real and Imaginary parts of the resolvent  $G(z)$  as a function of  $\text{Re}(z)$  and  $\text{Im}(z)$  for  $\text{Im}(z) = 0$  and  $\text{Re}(z) = 0$ , respectively.

simulations becomes extremely slow for  $\mu^2 n > 1$ . The average resolvent is the sum of terms weighted with a typical value of the determinant. Because of the normalization we expect an enhancement factor of  $\sim e^{n\mu^2}$ . The ratios of the maximum values of the real part of the resolvent in Figs. 4 and 6 are consistent with this enhancement factor.

## 8. Conclusions

We have studied the role of the fermion determinant in a random matrix model at nonzero chemical potential. Previously, it was shown by Stephanov that the quenched version of this model is given by the limit  $N_f \rightarrow 0$  of this partition function with the determinant replaced by its absolute value, and that, for example, the chiral condensate differs from the unquenched result. We have demonstrated that the equality of the valence and sea quark masses is of fundamental importance in arriving at a consistent partition function. A saddle point analysis was shown to be in complete agreement with an explicit calculation of the Yang-Lee zeros of the partition function which were found to be located on a curve in the complex plane. If the valence quark mass and the sea quark mass are different, the condensate can diverge if the mass is inside the domain of the eigenvalues. We have shown this analytically for the  $U(1)$ -model of Gibbs and numerically for the

random matrix model. The reason for this divergence is that, in the chirally broken phase, the partition function vanishes like  $\exp(-n\mu^2)$  in the thermodynamic limit.

While we do not expect that the random matrix model considered here leads to quantitative results, we believe that some of the generic features we have observed might be present in QCD as well.

### Acknowledgements

This work was partially supported by the US DOE grant DE-FG-88ER40388. We thank Robert Shrock for useful discussions and educating us on to general properties of Yang-Lee zeros. Misha Stephanov, Melih Şener and Gábor Papp are thanked for useful discussions. James Osborn is thanked for pointing out the existence of multiprecision packages. We acknowledge D.H. Bailey and NASA Ames for making their multiprecision package available.

Finally, we wish to point out that at the time of submission of this paper we received a preprint by J. Feinberg and A. Zee [21] with minor overlaps with the present work. In particular, parts of sections 2, 3.1 and 3.2 are also discussed in [21].

### REFERENCES

1. C. DeTar, *Quark-gluon plasma in numerical simulations of QCD*, in *Quark gluon plasma 2*, R. Hwa ed., World Scientific 1995.
2. A. Ukawa, Nucl. Phys. Proc. Suppl. **53** (1997) 106.
3. I. Barbour, S. Morrison and J. Kogut, hep-lat/9612012.
4. I. Barbour, N. Behihil, E. Dagotto, F. Karsch, A. Moreo, M. Stone and H. Wyld, Nucl. Phys. **B275** (1986) 296.
5. J.B. Kogut and M.P. Lombardo, Phys. Rev. **D 51** (1995) 1282; M.P. Lombardo, J.B. Kogut and D.K. Sinclair, Phys. Rev. **D 54** (1996) 2303.
6. F. Butler, H. Chen, J. Sexton, A. Vaccarino and D. Weingarten, Phys. Rev. Lett. **70** (1993) 2849.
7. N. Bilic and K. Demeterfi, Phys. Lett. **B212** (1988) 83.
8. J. Vink, Nucl. Phys. **B323** (1989) 399.
9. P.E. Gibbs, Phys. Lett. **B172** (1986) 53.
10. P.E. Gibbs, Phys. Lett. **B182** (1986) 369.

11. A. Gocksch, Phys. Rev. Lett. **61** (1988) 2054.
12. M. Stephanov, Phys. Rev. Lett. **76** (1996) 4472.
13. M.F.L.Golterman, Acta Phys. Polon. **B25** (1994) 1731.
14. S.J. Hands and M. Teper, Nucl. Phys. Proc. Suppl. **42** (1995) 237.
15. P.H.Damgaard, N.Kawamoto, K.Shigemoto, Nucl. Phys **B264** (1986) 1.
16. P.H. Damgaard, D. Hochberg and N. Kawamoto, Phys. Lett. **158B** (1985) 239.
17. E.V. Shuryak and J.J.M. Verbaarschot, Nucl. Phys. **A560** (1993) 306; J.J.M. Verbaarschot, Phys. Rev. Lett. **72** (1994) 2531; Phys. Lett. **B329** (1994) 351; Nucl. Phys. **B427** (1994) 434; J.J.M. Verbaarschot and I. Zahed, Phys. Rev. Lett. **70** (1993) 3852.
18. J.J.M. Verbaarschot, Nucl. Phys. Proc. Suppl. **53** (1997) 266.
19. M. Halasz, A. Jackson and J. Verbaarschot, Phys. Lett. **B** (1997) (in press).
20. J.J.M. Verbaarschot, H.A. Weidenmüller and M.R. Zirnbauer, Phys. Rep. **129** (1985) 367; H.J. Sommers, A. Crisanti, H. Sompolinsky and Y. Stein, Phys. Rev. Lett. **60** (1988) 1895; F. Haake, F. Izrailev, N. Lehmann, D. Saher, and H.J. Sommers Z. Phys. B88 (1992) 359; R.A. Janik, M. A. Nowak, G. Papp, J. Wambach and I. Zahed, hep-ph/9609491; R.A. Janik, M. A. Nowak, G. Papp, and I. Zahed, hep-ph/9612240; Y. Fyodorov, B.A. Khoruzhenko and H.J. Sommers, cond-mat/9606173.
21. J. Feinberg and A. Zee, cond-mat/9703087.
22. V.Matveev and R.Shrock, J.Phys A: Math Gen.**28** (1995) 1557, 4859; Phys. Rev. **E** **53** (1996) 254.
23. A.D.Jackson and J.J.M.Verbaarschot, Phys. Rev. D**53** (1996) 7223.
24. T. Wettig, A. Schäfer and H. Weidenmüller, Phys. Lett. **B367** (1996) 28.
25. M. Stephanov, Phys. Lett. **B275** (1996) 249.
26. A.D Jackson, M.K. Sener and J.J.M. Verbaarschot, Nucl. Phys. **B479** [FS] (1996) 707.
27. J. Ginibre, J. Math. Phys **6** (1965) 440.
28. D.H. Bailey, *A Fortran-90 Based Multiprecision System* , NASA Ames RNR Technical Report RNR-94-013
29. M.A. Stephanov, Nucl. Phys. Proc. Suppl. **53** (1997) 469.